# Supporting Information

# Promoting Effect of $Cu^{2+}$ Ions on Electrochemical Ammonia Oxidation Using CuO Electrocatalysts

*Taerin Kim [a,‡], Hyun Ji An [a,‡], Jiwon Jeon [b,‡], Eunchong Lee [a], Sang Heon Han [a], Hyeyoung Shin [b,]*, and Yun Jeong Hwang [a,]**

[a]Department of Chemistry, Seoul National University, Seoul 08826, Republic of Korea

[b]Graduate School of Energy Science and Technology, Chungnam National University, Daejeon 34134, Republic of Korea

[‡]These authors contributed equally.

* shinhy@cnu.ac.kr; yjhwang1@snu.ac.kr

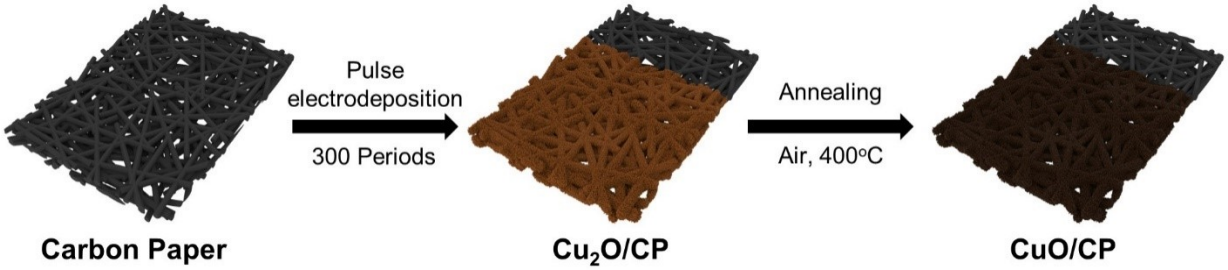


**Figure S1.** Scheme for CuO/CP synthesis. Each period of pulse electrodeposition was conducted by applying -0.467 V (*vs.* Ag/AgCl) for 2 s and sequentially applying 0.033 V (*vs.* Ag/AgCl) for 4 s.

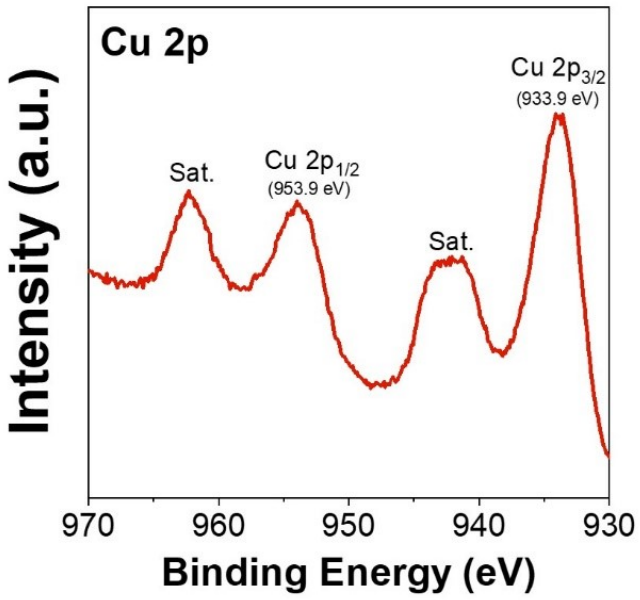


**Figure S2.** Cu 2p XPS spectrum of CuO/CP showing characteristic features corresponding to Cu(II)O.

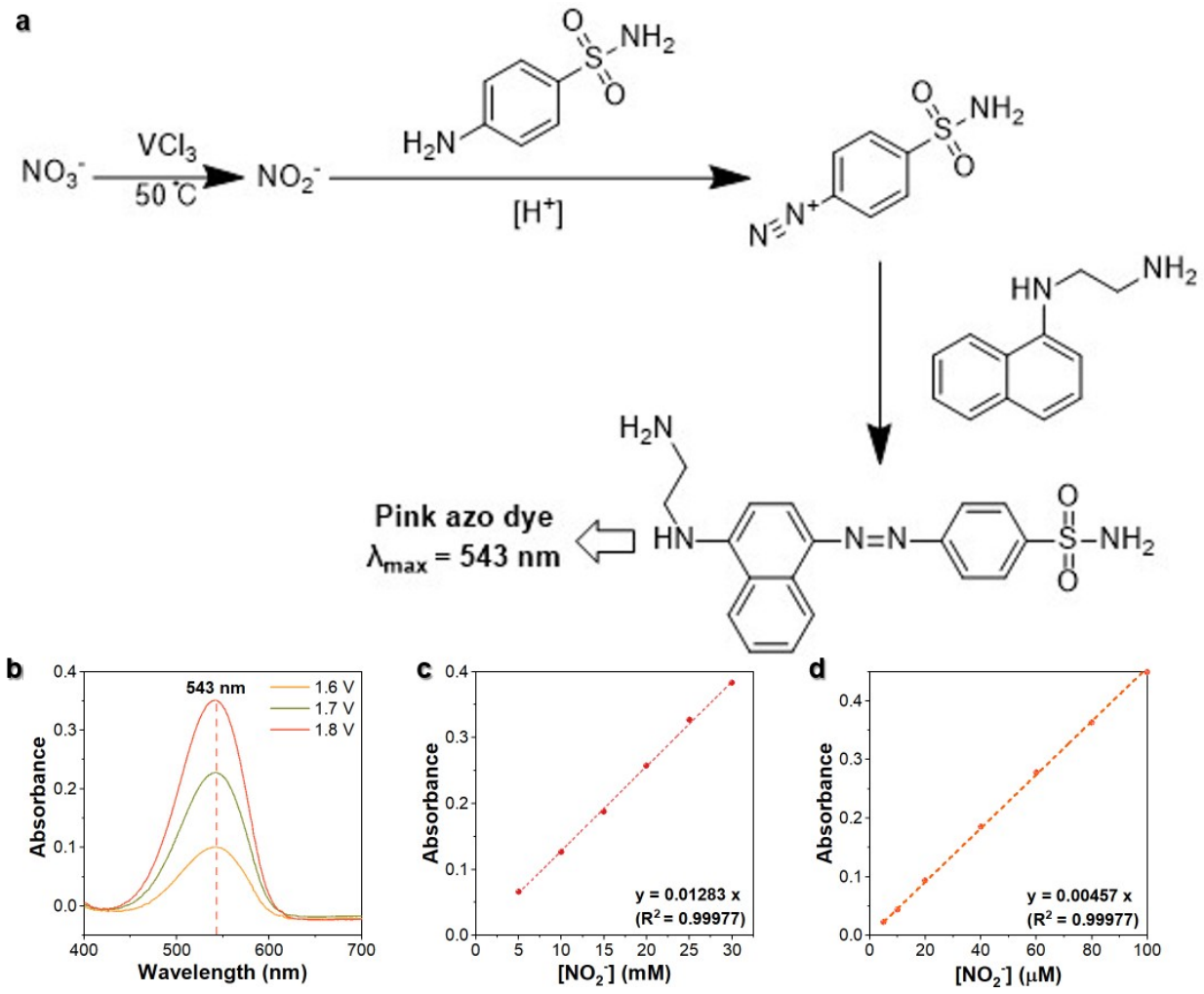


**Figure S3.** Griess assay for $NO_x^-$ ions quantification by UV–vis spectroscopy (a) Reaction scheme of $NO_x^-$ species and Griess reagent to produce a pink azo dye. (b) UV–vis spectra after eAOR with CuO/CP anode at 1.6, 1.7, and 1.8 V *vs.* RHE, respectively. Calibration curve taken with standard $NO_2^-$ solution between (c) 5 to 30 mM, and (d) 5 to 100 μM.

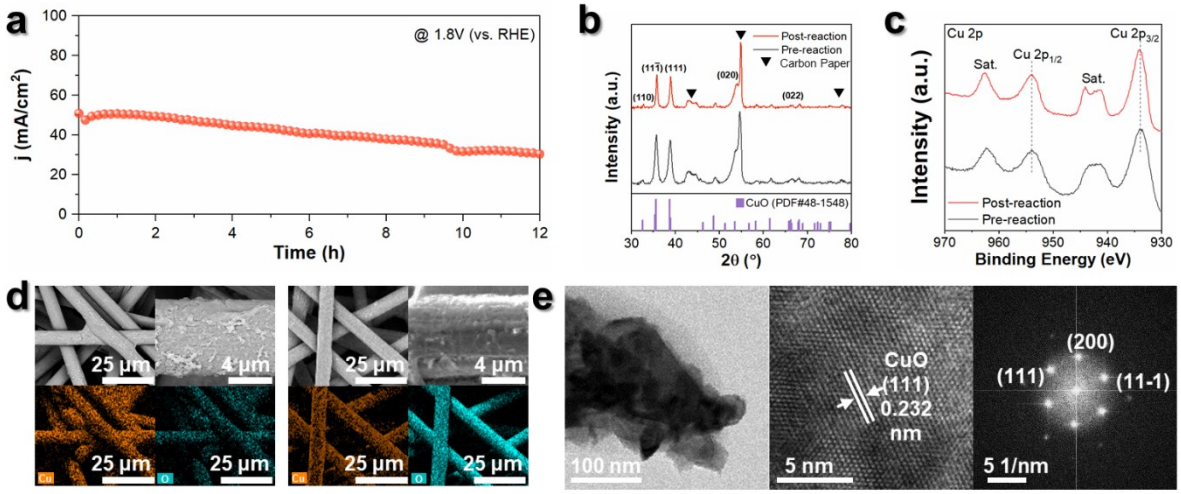


**Figure S4.** (a) Chronoamperometry measurement of CuO/CP electrode obtained at 1.8 V (*vs.* RHE) under 1 M KOH + 0.5 M $NH_3$ for 12 h. Post-reaction CuO/CP electrode in this figure was obtained at 1.8 V (*vs.* RHE) under 1 M KOH + 0.5 M $NH_3$ for 12 h. (b) XRD, and (c) XPS for pre- (black line) and post-reaction (red line) CuO/CP. (d) SEM-EDS image of pre- (left) and post-reaction (right) electrode. (e) Low magnification, HR-TEM lattice fringe image, and SAED patterns of post-reaction CuO/CP

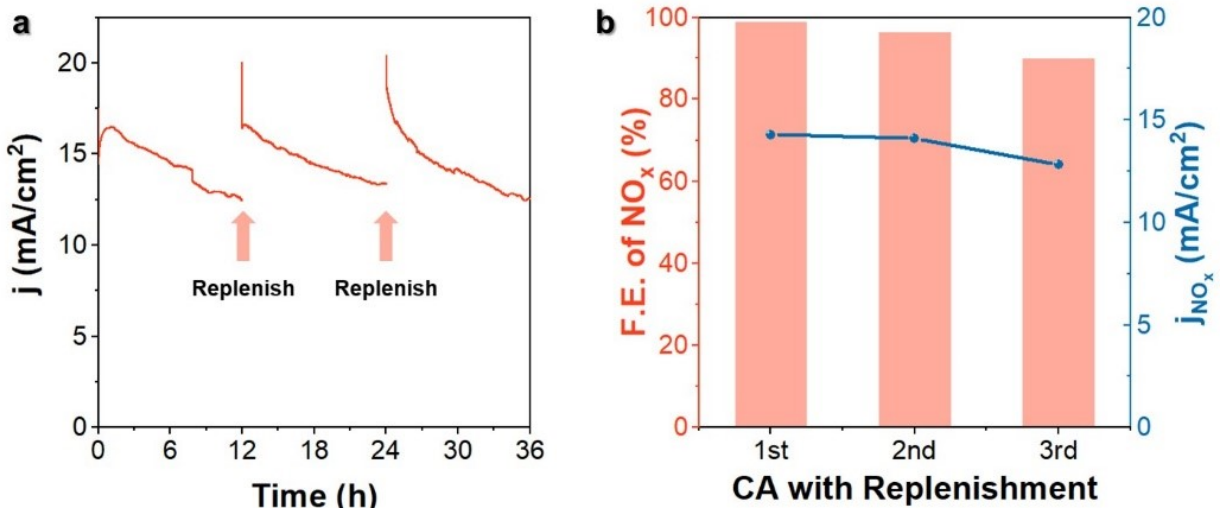


**Figure S5.** (a) Chronoamperometry (CA) measurement at 1.6 V (*vs.* RHE) with CuO/CP catalysts under 1 M KOH and 0.5 M $NH_3$. Electrolyte was replenished every 12 h. (b) F.E. of $NO_x^-$ and $j_{NOx}$ for each 12 h reaction in (a)

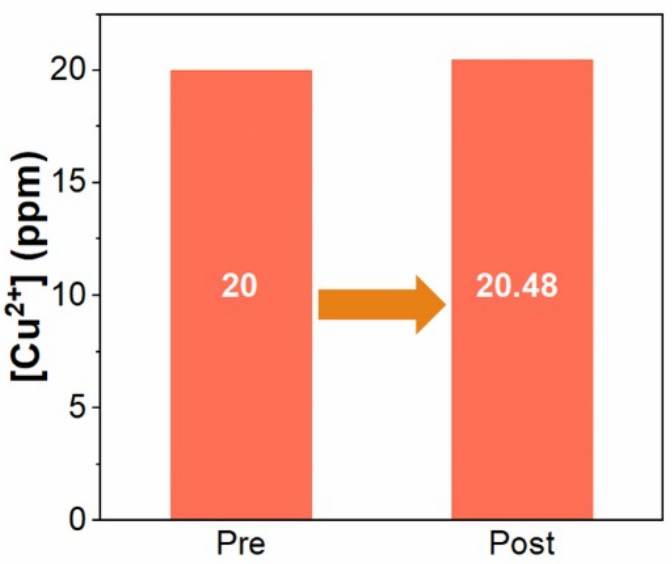


**Figure S6.** $Cu^{2+}$ concentration measured by ICP-OES of pre- and post-reaction electrolyte of eAOR with CuO/CP electrode, applying 1.6 V (*vs.* RHE) for 12 h in the 20 ppm of $Cu^{2+}$ added 1 M KOH and 0.5 M $NH_3$ electrolyte.

s

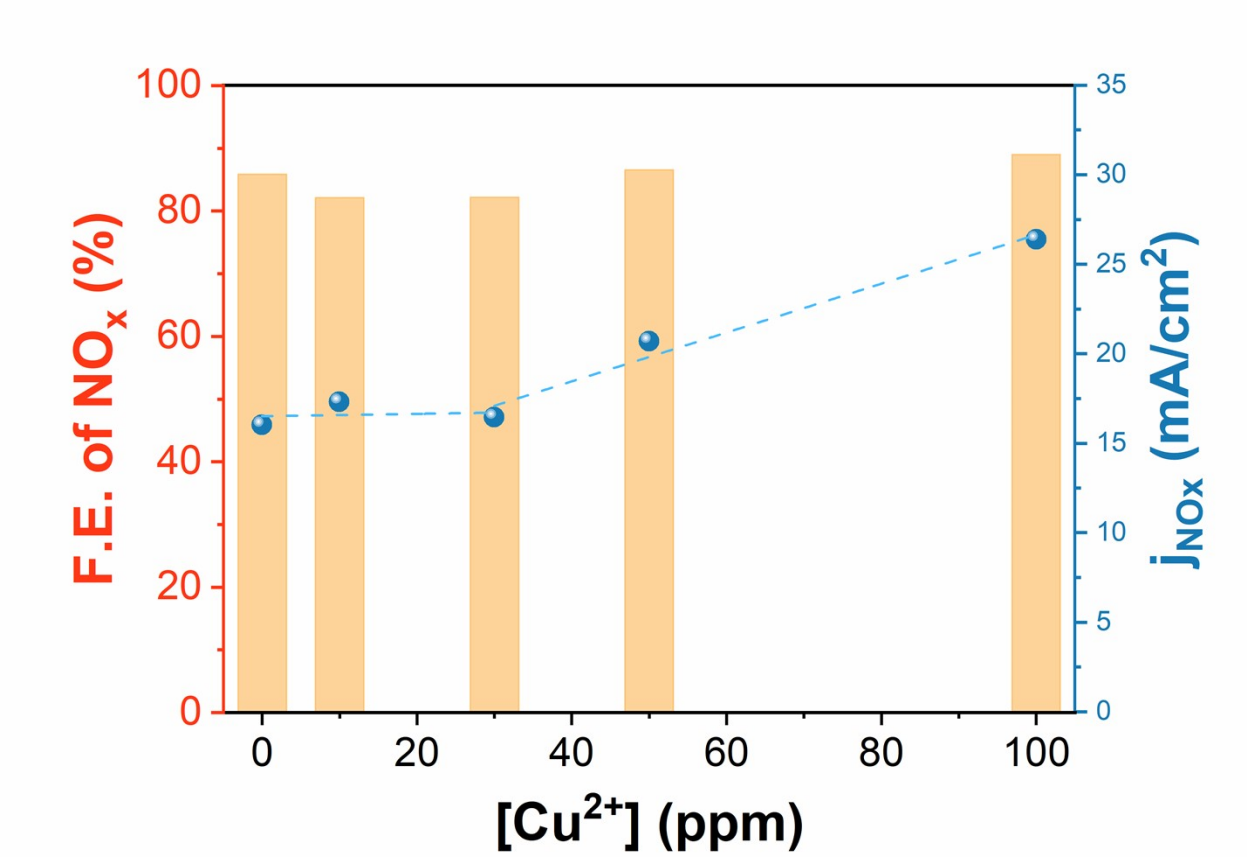


**Figure S7.** F.E. of $NO_x$ and $j_{NOx}$ for the eAOR at 1.6 V (*vs.* RHE) with CuO/CP electrode at 1 M KOH with 0.5 M $NH_3$ electrolyte in the presence of *x* ppm (*x* = 0, 10, 30, 50, 100) $Cu^{2+}$ ions. For all experiments, $Cu^{2+}$ ions were dissolved in the electrolyte before the potential was applied.

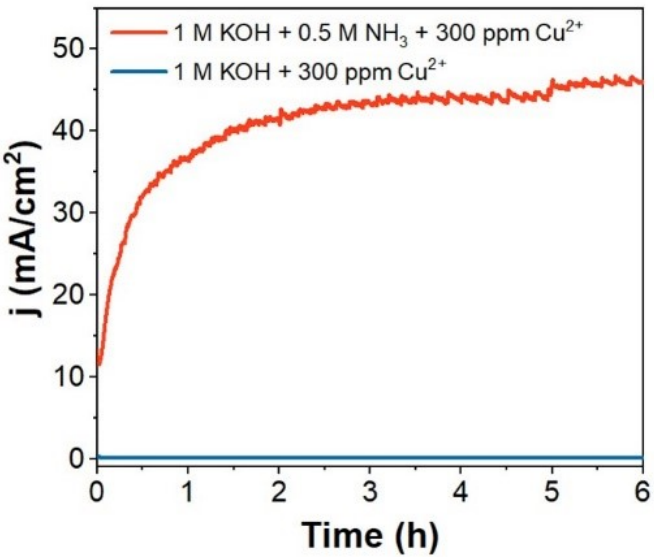


**Figure S8.** Chronoamperometry measurement of bare carbon paper anode obtained at 1.8 V (*vs.* RHE) under 1 M KOH + 0.5 M $NH_3$ (red line) and 1 M KOH (blue line) in the presence of 300 ppm $Cu^{2+}$.

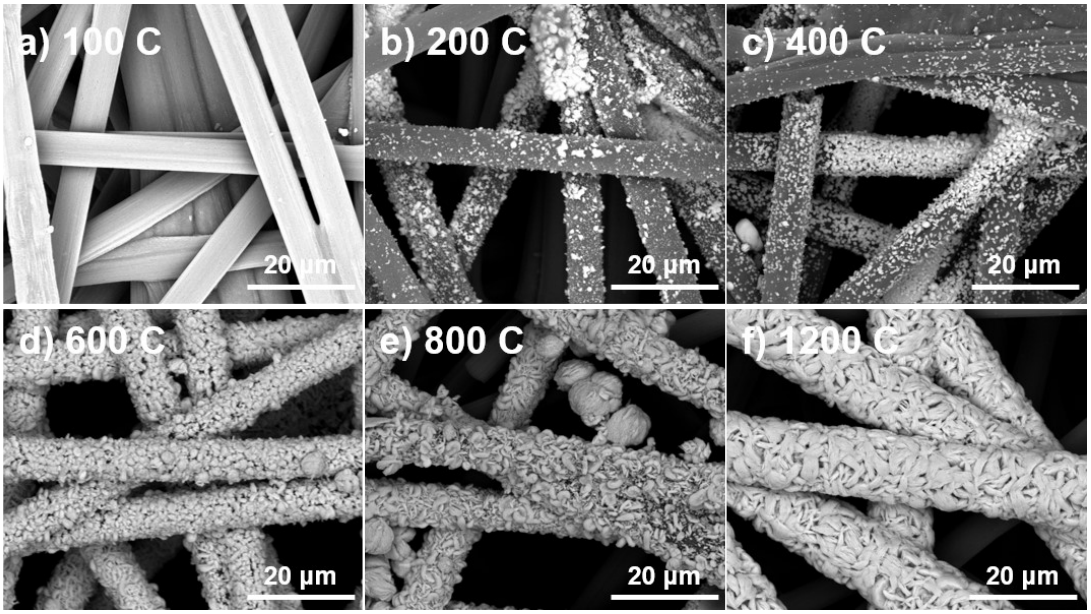


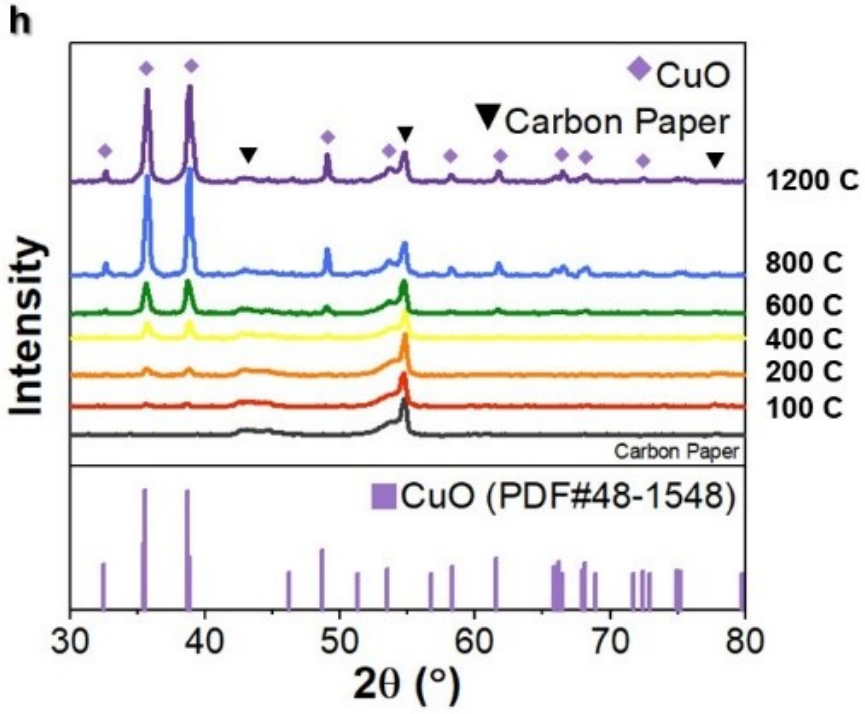


**Figure S9.** SEM image of carbon paper anode after applying 1.8 V (*vs.* RHE) 1 M KOH and 0.5 M $NH_3$ in the presence of 300 ppm $Cu^{2+}$. Each image was obtained from (a) 100 C, (b) 200 C, (c) 400 C, (d) 600 C, (e) 800 C, and (f) 1200 C, respectively. (h) XRD spectra from (a) to (f).

**Table S1.** Amount of Cu deposited on carbon paper applying 1.8 V (*vs.* RHE) under 1 M KOH and 0.5 M $NH_3$ in the presence of 300 ppm $Cu^{2+}$

| Passed charge (C) | Time (s) | Deposited Cu (mg) | Ratio of deposited Cu (%) |
|---|---|---|---|
| 100 | 2296.26 | 0.04122 | 0.9160 |
| 200 | 4784.24 | 0.1362 | 3.071 |
| 400 | 7979.91 | 0.3972 | 8.827 |
| 600 | 11892.2 | 0.8876 | 19.72 |
| 800 | 17890.6 | 2.19875 | 48.86 |
| 1200 | 26608.9 | 2.5695 | 57.10 |

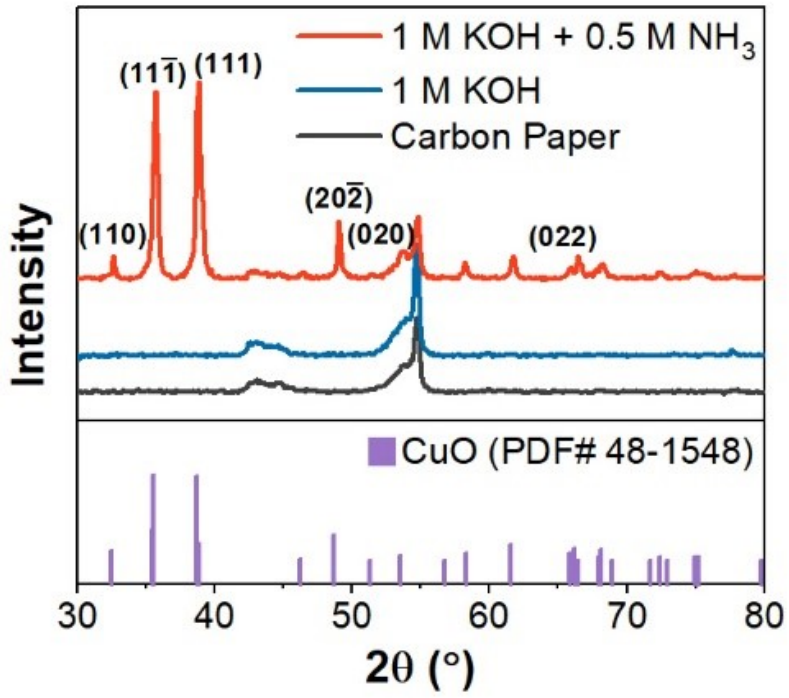


**Figure S10.** XRD spectra of carbon paper anode obtained after applying 1.8 V (*vs.* RHE) under 1 M KOH and 0.5 M $NH_3$ (red line) and 1 M KOH (blue line) in the presence of 300 ppm $Cu^{2+}$, showing that CuO was only deposited in the case of 1 M KOH and 0.5 M $NH_3$. Black data shows the XRD spectrum of bare carbon paper.

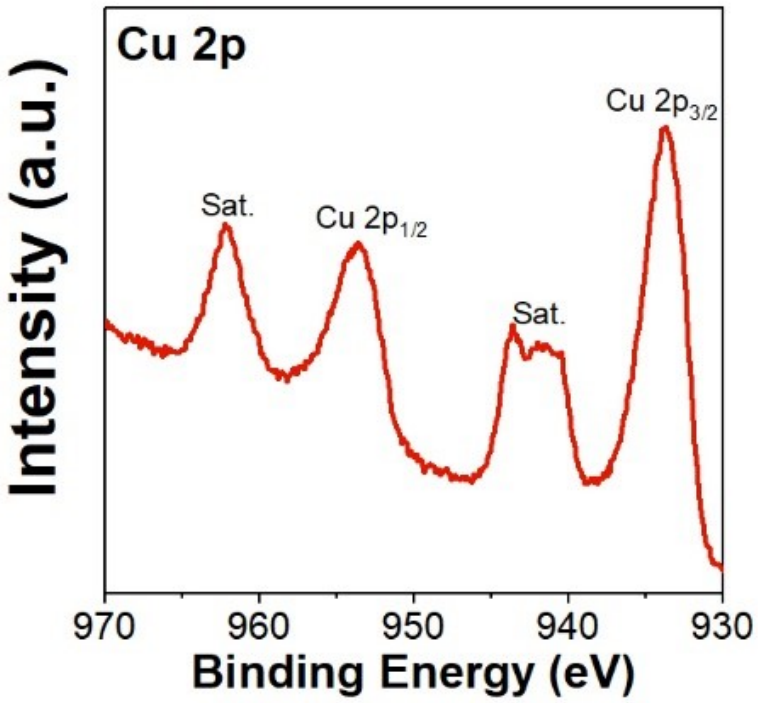


**Figure S11.** Cu 2p XPS spectrum of carbon paper anode obtained after applying 1.8 V (*vs.* RHE) under 1 M KOH + 0.5 M $NH_3$ in the presence of 300 ppm $Cu^{2+}$, showing characteristic features corresponding to Cu(II)O.

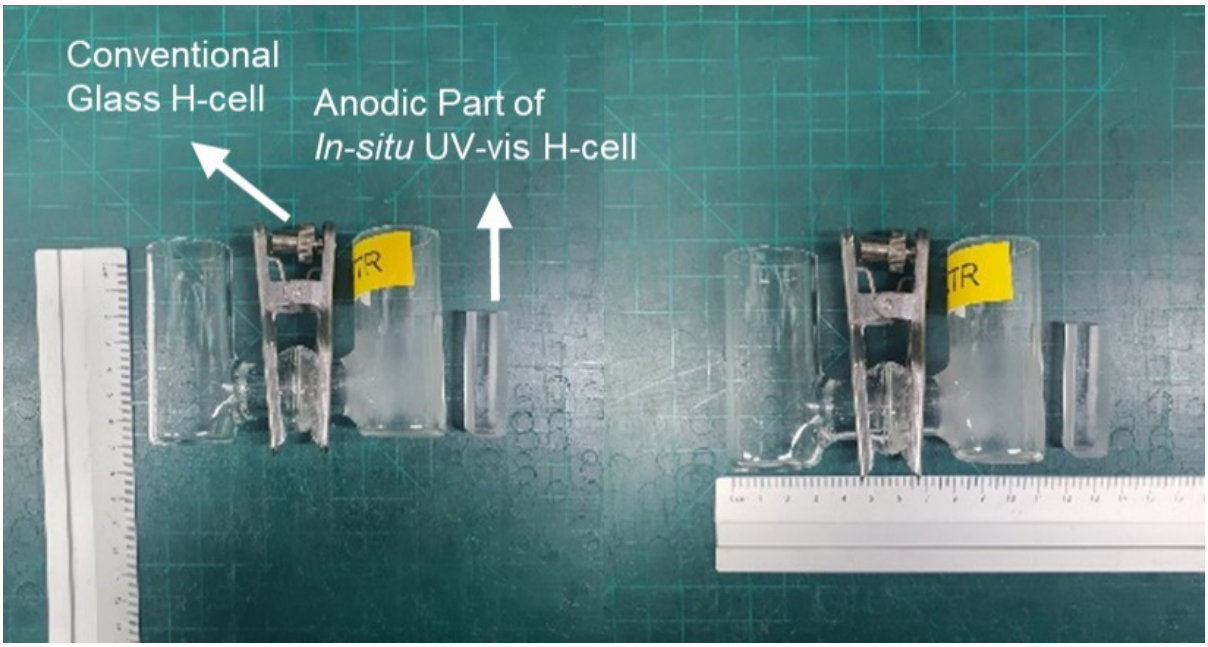


**Figure S12.** The photographic images of the conventional glass H-Cell and the anodic part of the *in situ* UV-vis H-Cell.

The $Cu^{2+}$ concentration was also measured with ICP-OES after applying 1.8 V (*vs.* RHE) for 120 min to the CuO/CP in an *in situ* UV-vis H-cell. Although there existed a discrepancy for the equilibration time to reach the saturation of $Cu^{2+}$ ions between experiments with the *in situ* UV-vis H-cell (Figure 3f) and a conventional glass H-cell (Figure 1e), due to the volume of electrolyte, the $Cu^{2+}$ concentration after reaching a plateau was similar (14.4 ± 4.8 ppm for the *in situ* UV-vis H-cell experiment and 15.8 ppm for the conventional glass H-cell experiment, corresponding to the result of Figure 1e, respectively).

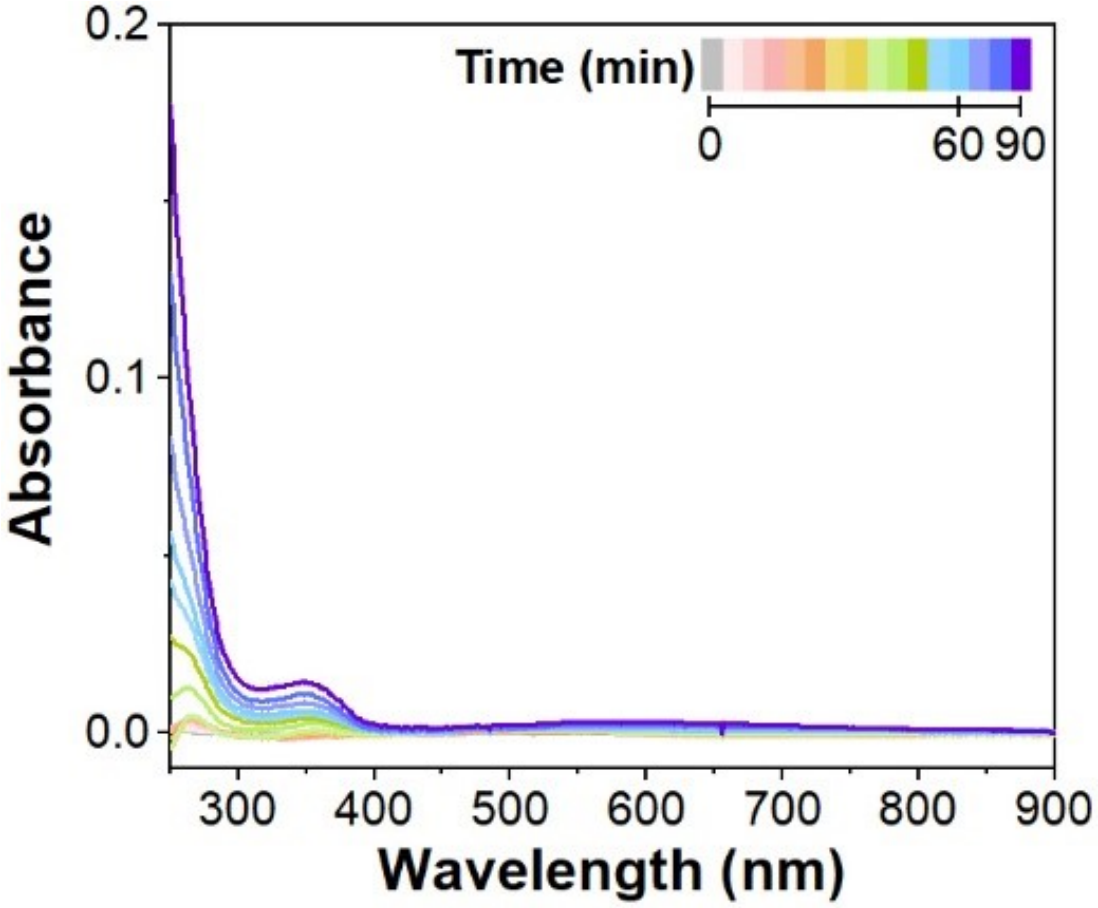


**Figure S13.** *In situ* UV–vis spectra of carbon paper applying 1.8 V (*vs.* RHE) under 1 M KOH and 0.5 M $NH_3$ without $Cu^{2+,}$ showing that both $NO_2^-$ and $NO_3^-$ formation are negligible.

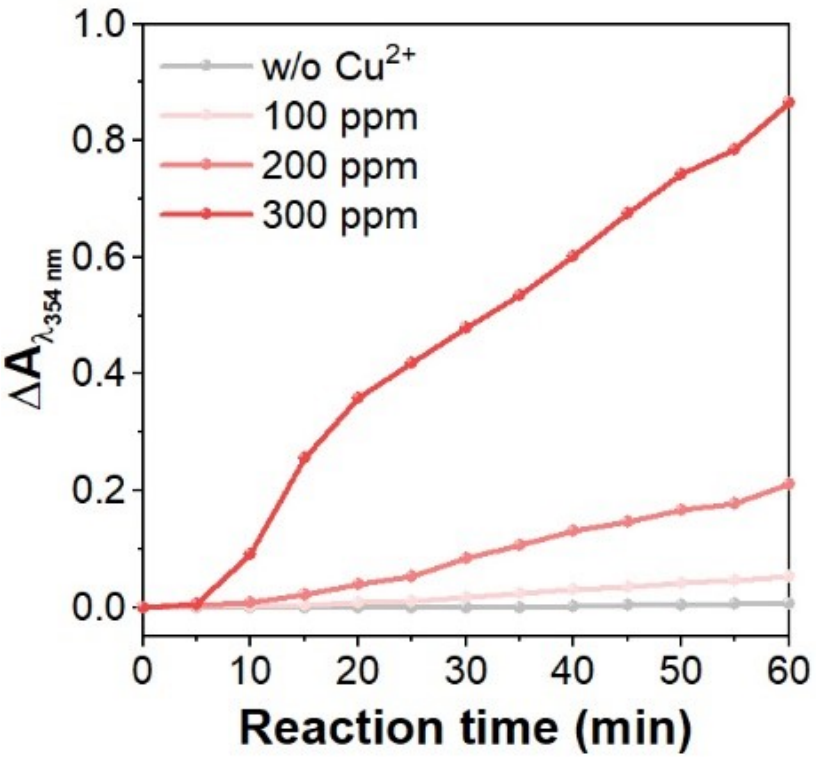


**Figure S14**. Absorbance change at λ = 354 nm for *in situ* H-Cell UV–vis for carbon paper applying 1.8 V (*vs.* RHE) under 1 M KOH and 0.5 M $NH_3$ in the presence of different concentrations of $Cu^{2+}$, supporting that $Cu^{2+}$ is an active reactant for $NO_2^-$-selective AOR.

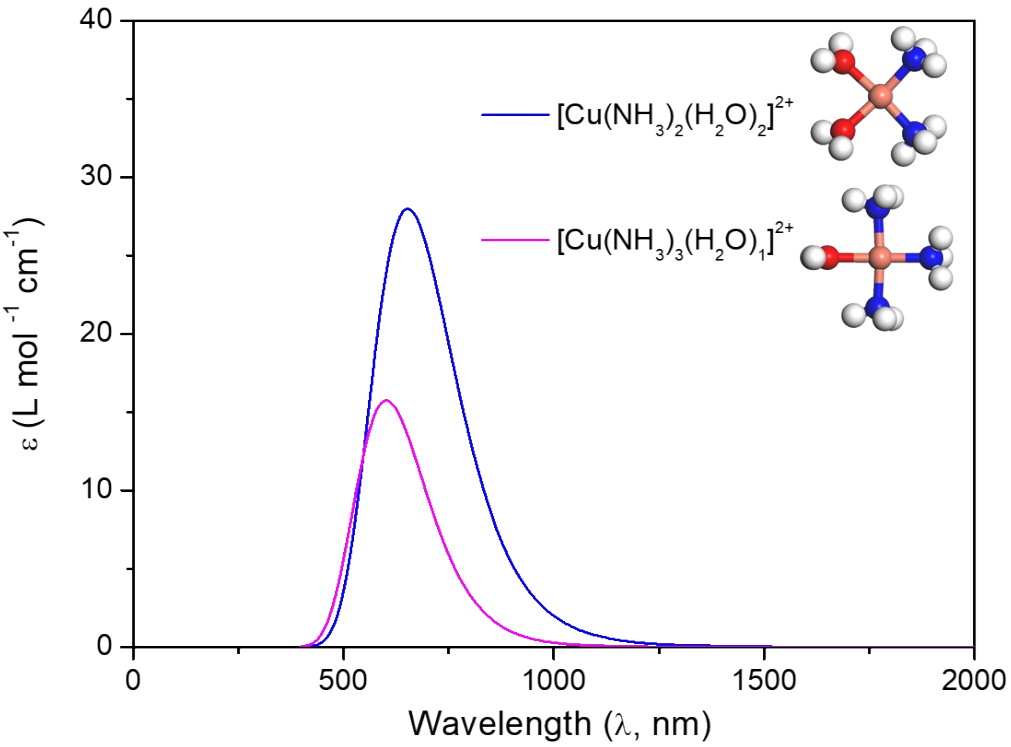


**Figure S15.** UV-vis absorption spectra obtained from TD-DFT calculations and the corresponding optimized geometries of $[Cu(NH_3)_2(H_2O)_2]^{2+}$ and $[Cu(NH_3)_3(H_2O)]^{2+}$ complexes. Cu (orange), N (blue), H (white), and O (red).

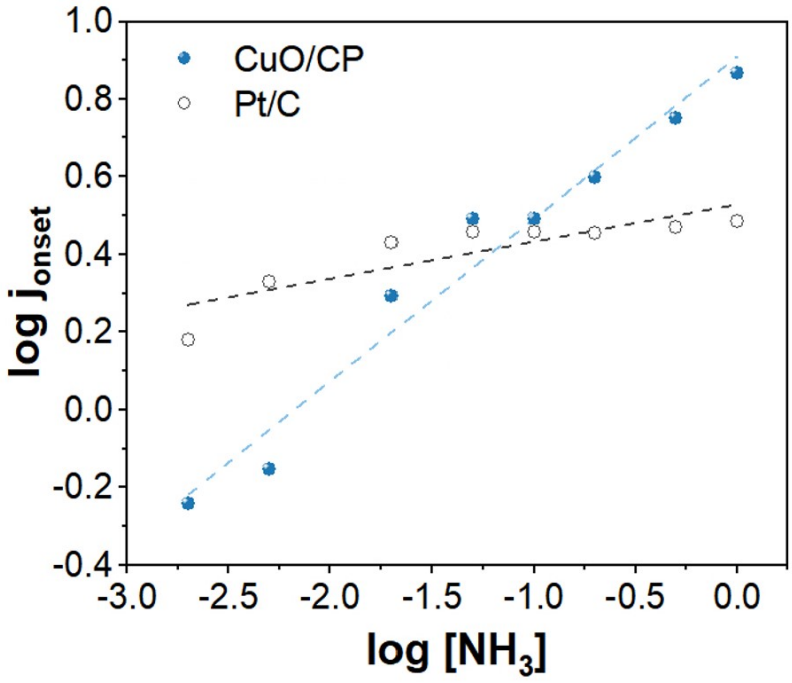


**Figure S16.** $NH_3$ concentration dependence of current density near the onset potential ($j_{onset}$) for Pt/C (Black) and CuO/CP (Blue). Cyclic voltammetry was conducted under 1 M KOH and *x* mM $NH_3$ electrolytes (*x* = 2, 5, 10, 20, 50, 100, 200, 500, and 1000). $J_{onset}$ data were collected at 0.57 V (*vs.* RHE) for Pt/C (slope 0.076, $R^2 = 0.7066$) and 1.50 V (*vs.* RHE) for CuO/CP (slope 0.42, $R^2 = 0.96023$)

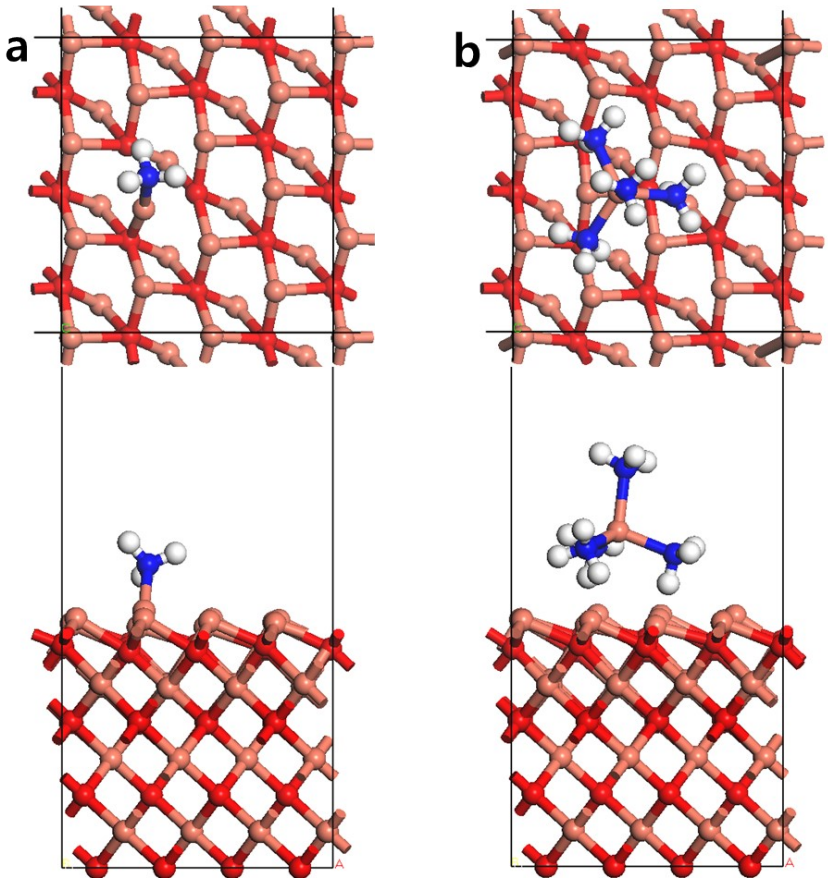


**Figure S17.** DFT-optimized structures of (a) a single $NH_3$ molecule and (b) a $[Cu(NH_3)_4]^{2+}$ complex adsorbed on the CuO (002) surface. Cu (orange), N (blue), H (white), and O (red).

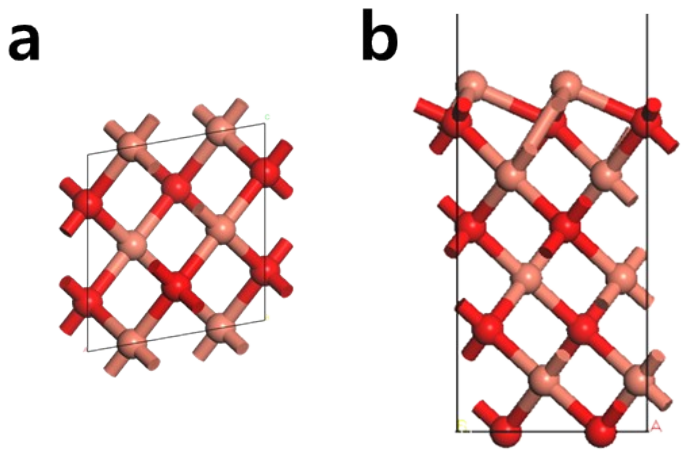


**Figure S18.** DFT-optimized structures of (a) bulk CuO and (b) CuO (002) surface. Cu (orange), and O (red).

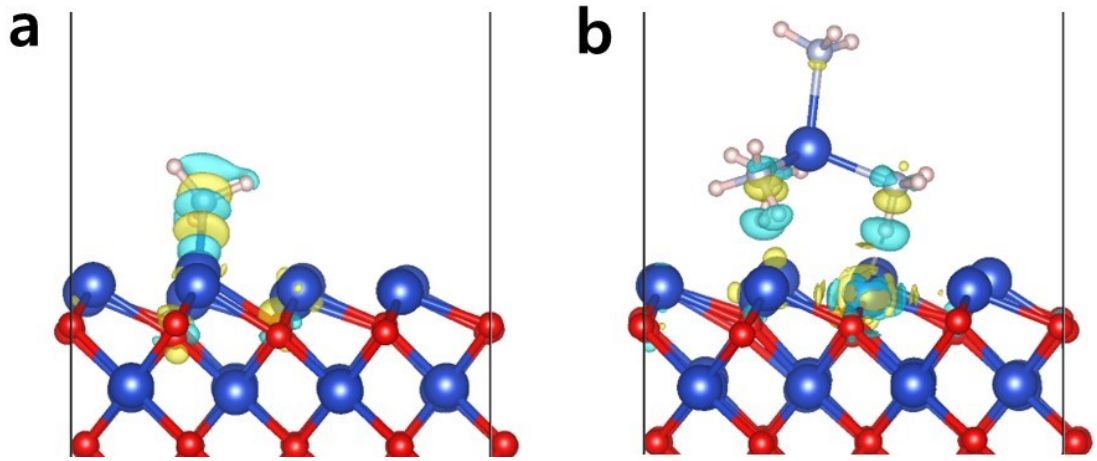


**Figure S19.** Charge density difference ($\Delta\rho$) maps for (a) $NH_3$ and (b) $[Cu(NH_3)_4]^{2+}$ adsorbed on the CuO (002) surface. Yellow and cyan regions represent electron accumulation and depletion, respectively. The isosurface value is set to 0.003 e/Å$^3$.

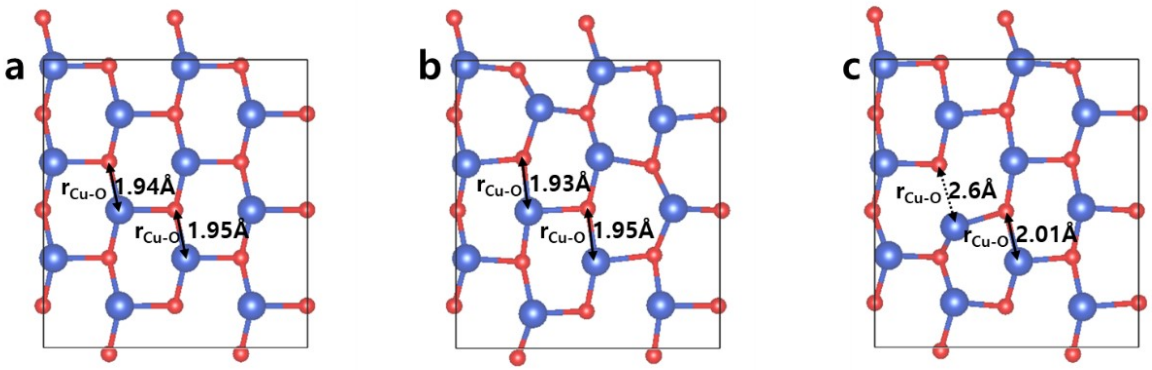


**Figure S20.** Top views of DFT-optimized CuO (002) surface structures: (a) bare surface, (b) $[Cu(NH_3)_4]^{2+}$-adsorbed surface, and (c) $NH_3$-adsorbed surface.

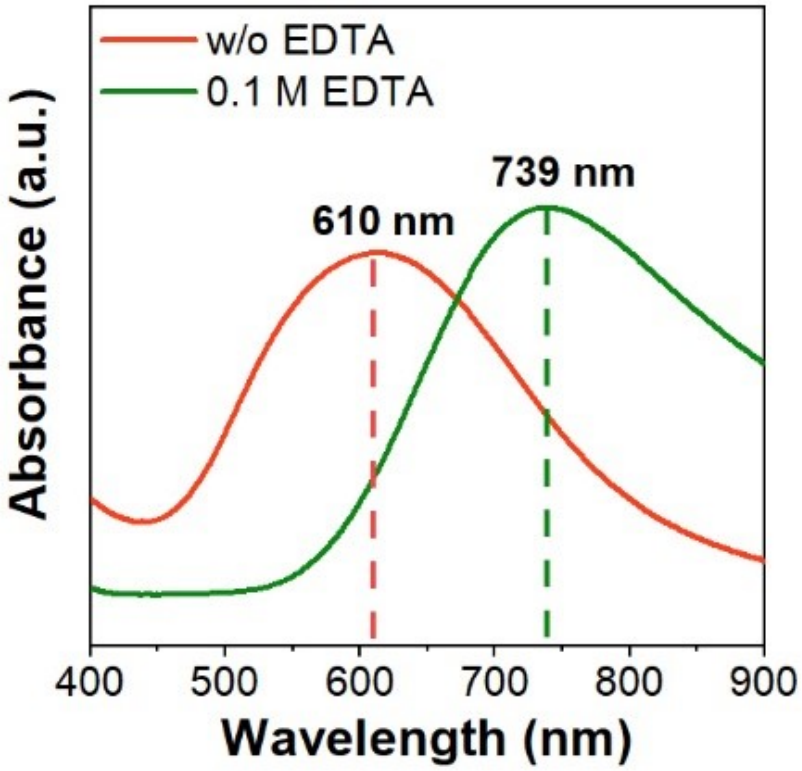


**Figure S21**. UV–vis absorption spectra of $Cu^{2+}$ with (green line) and without (red line) EDTA under 1 M KOH and 0.5 M $NH_3$, showing that $Cu^{2+}$ exists as a different complex in the two electrolytes.

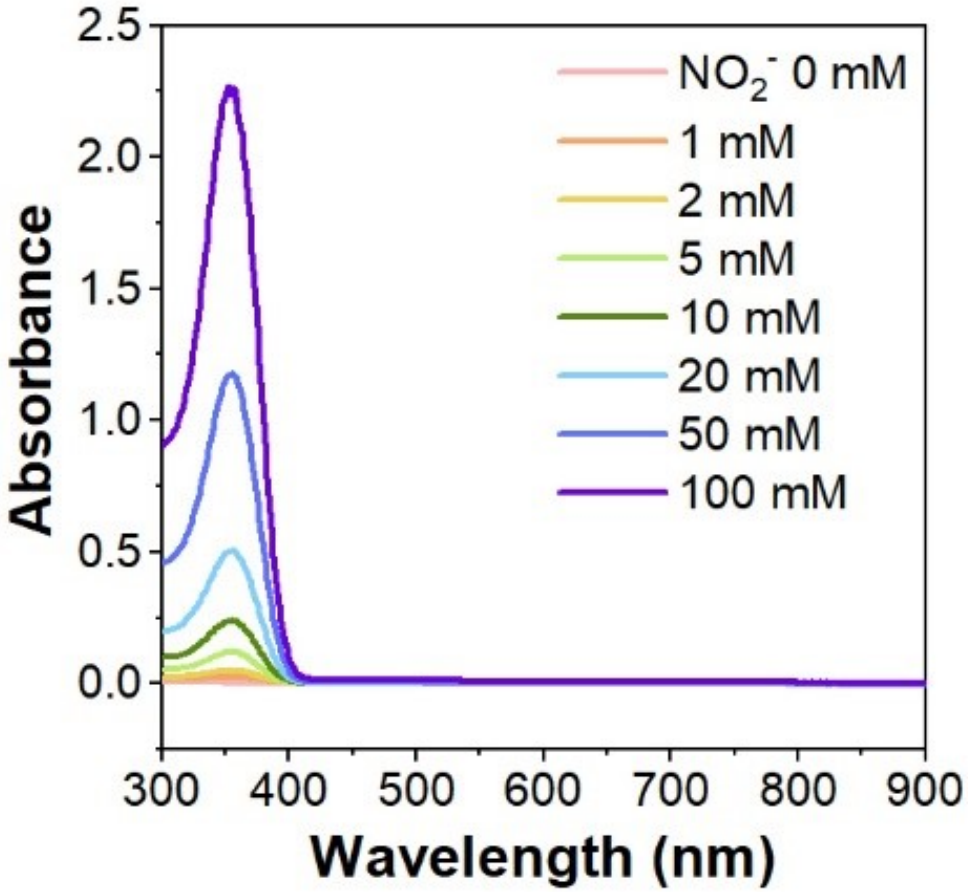


**Figure S22.** *Ex situ* UV–vis spectra of $NO_2^-$ under 1 M KOH and 0.5 M $NH_3$ in the presence of 0.1 M EDTA, showing that the $NO_2^-$ adsorption peak is not diminished in the presence of EDTA.

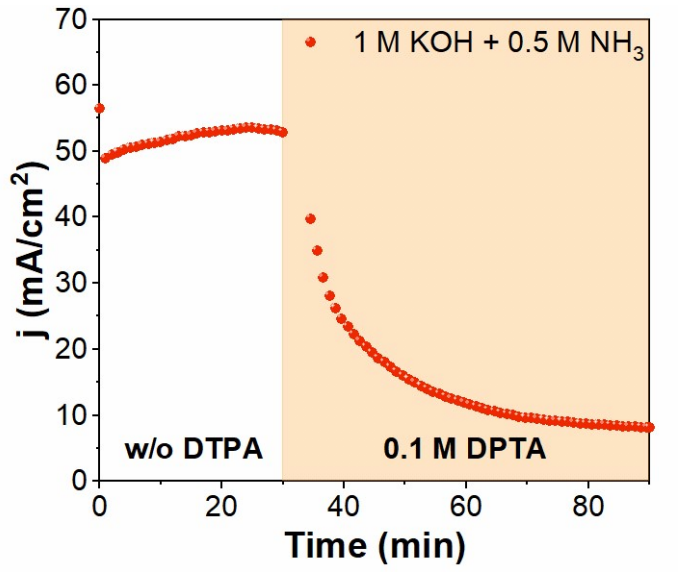


**Figure S23.** Chronoamperometry measurement of the CuO/CP electrode depending on the 0.1 M DTPA addition at 1.8 V (*vs.* RHE) in 1 M KOH with 0.5 M $NH_3$. 0.1 M of DTPA was spiked into the electrolyte in the middle of the reaction.

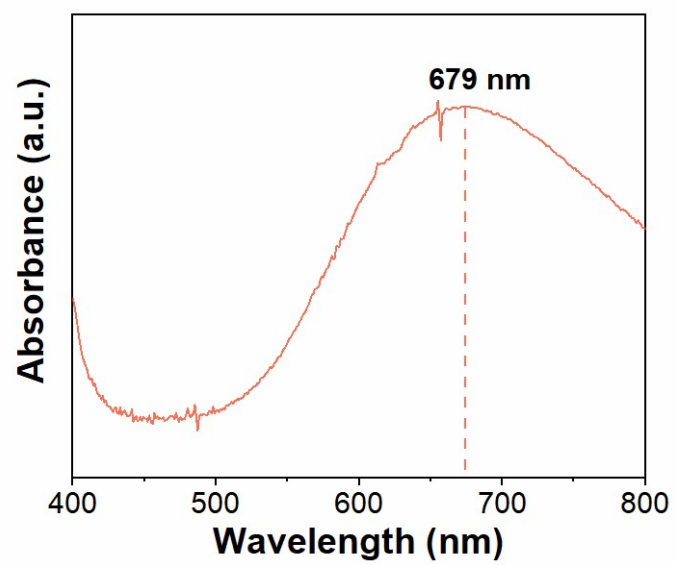


**Figure S24.** *Ex situ* UV-vis absorption spectrum of post-reaction electrolyte of eAOR with CuO/CP electrode at 1 M KOH and 0.5 M $NH_3$ in the presence of 0.1 M DTPA.